

# A METHOD FOR NARROW FIELD-OF-VIEW REGION-OF-INTEREST COMPUTED TOMOGRAPHY

Esmail Enjilela and Esam M. A. Hussein

Laboratory for Threat Material Detection, Department of Mechanical Engineering  
University of New Brunswick, P.O. Box 4400, Fredericton NB, E3B 5A3, Canada  
Email:ltmd@unb.ca

## ABSTRACT

This paper presents a method for reconstructing of an internal tomographic image for a region-of-interest (RoI) within a section, using narrowed radiation beams. This reduces radiation exposure, and with the aid of an iterative image reconstruction algorithm, RoI images are reconstructed with a quality comparable to conventional computed tomography (CT) full field-of-view images. Region-of-interest image reconstruction is formulated as a discrete problem to avoid the truncated (incomplete) problem associated with the conventional analytic filtered backprojection method. This in turn allows local reconstruction of RoI images without any prior information or constraints. A coarse image of the entire section is first reconstructed with the aid of a modified convex maximum likelihood (MCML) algorithm. The coarse image is then used to account for the effect of the RoI surroundings. With RoI-specific projections, an RoI image is then reconstructed with the MCML method at the desired pixel size. The proposed method is evaluated using an anthropomorphic thorax phantom, with the heart as its RoI, showing an image quality comparable to that of a conventional CT, but with a about 72% reduction in radiation exposure. Unlike existing approaches that require some a priori knowledge of a segment of the image, this approach does not require any prior image information or any constrains on the solution.

## INTRODUCTION

There is a desire to reduce patient exposure to radiation during computed tomography (CT) scanning, particularly when there is a need to image a particular region-of-interest (RoI) in the body. Such localized imaging can be accomplished by confining radiation exposure to the RoI using a narrow field-of-view (FoV)

beam aimed at the RoI, contrary to the full FoV employed in conventional CT. However, when viewed analytically in the continuous domain, required for the Fourier transforms of the widely used filtered backprojection (FBP) method, the problem becomes incomplete, due to the truncation of its projections outside the RoI. Attempts have been made to solve this truncated-projection problem by utilizing some supplementary information [1,2], such as object's outline or an already available full-section image of the object. Some *a priori* knowledge about the nature of surrounding materials [3,4] and solution constraints [5,6] were also utilized to solve this truncated problem. In practice, such requirements are not always attainable. In this work, we liberate the RoI image reconstruction problem from these requirements, by utilizing a discrete formulation of the problem, which allows local reconstruction of RoI images, without any prior image information or constraints.

## APPROACH

In a narrow FoV beam configuration directed to an RoI and rotating within a 360° angular range, radiation has to traverse the regions outside the RoI, and hence carry information on the RoI's surroundings. This provides an opportunity to account for the effect of material outside the RoI. This can be accomplished by reconstructing a full section image from the narrowed FoV exposure. Since there are a limited number of ray-sums available in the narrow FoV configuration, a larger pixel size has to be utilized in reconstructing the full section image. In this study, the size of the coarse pixel was determined so that the degree of overdetermination (ratio of the number of measurements to the number of pixels) was equal to at least three, as is the case in conventional FoV imaging [7]. In reconstructing

the coarse image, the widely used FBP method is avoided, because it would produce inaccurate image parameters and bright peripheral band artifact [5], due to the uneven measurement sampling associated with the narrow FoV exposure. Matrix-based methods are better suited for such coarse imaging, given the fact that the interest here is not in obtaining a detailed full section image, but to account for the integral effect of the material outside the RoI. Iterative matrix-based methods, such as the conjugate gradient method or probabilistic methods are well suited for matrix-based image reconstruction. For ease of implementation, we have used of a modified convex maximum likelihood (MCML) algorithm [8]. Furthermore, the MCML algorithm is fast, guaranteed to converge to a solution, and preserves the expected non-negativity of the solution.

Once the coarse full-section image is reconstructed, its attributes (pixel attenuation coefficients) are used to account for the effect of the material surrounding the RoI on the measured rays-sums. The result is RoI-specific projections that can be used to reconstruct an RoI image with a pixel size equal to that typically used in medical applications. RoI image reconstruction is again formulated as a discrete problem, to take advantage of high signal-to-noise ratio of iterative image reconstruction algorithms. We have also employed the MCML algorithm for RoI image reconstruction, owing to its low susceptibility to error propagation and its ability to preserve the non-negativity of the reconstructed attenuation coefficients.

## SIMULATION RESULTS

The numerical schemes introduced in this work were tested by simulating a typical third generation CT system using the image reconstruction toolbox of [8]. This system had a 541 mm source-to-center of object distance and 949 mm source-to-detector distance. A thorax phantom, shown in Fig. 1, and emulating the lungs, heart, aorta, ribs, spine, and sternum, was simulated. The phantom was placed within a square with a width of 512 mm [11]. A circular RoI, shown in Fig. 1, with a diameter of 124 mm was considered. This RoI includes the aorta, vertebra and part of the

heart. This RoI was assumed to be exposed to a narrow FoV radiation within a  $15.3^\circ$  fan-beam so that it covered the entire RoI's 124 mm width from all  $360^\circ$  directions. A total of 218,700 ray-sums were synthesized, and then contaminated with 5% Gaussian, approximating the Poisson noise, typically encountered in conventional CT [9]. This number of ray-sums is only 27.36% of ray-sums required in a typical full FoV reconstruction, resulting in 72.64% reduction in radiation exposure. With this number of ray-sums, and aiming at the conventional degree of overdetermination of about three, a pixel size of  $1 \times 1 \text{ mm}^2$  can be used in reconstructing the RoI image, while the full-section image can only be reconstructed with coarser  $2 \times 2 \text{ mm}^2$  pixels. The  $1 \times 1 \text{ mm}^2$  pixel size is typical in full FoV medical imaging of thorax [7].

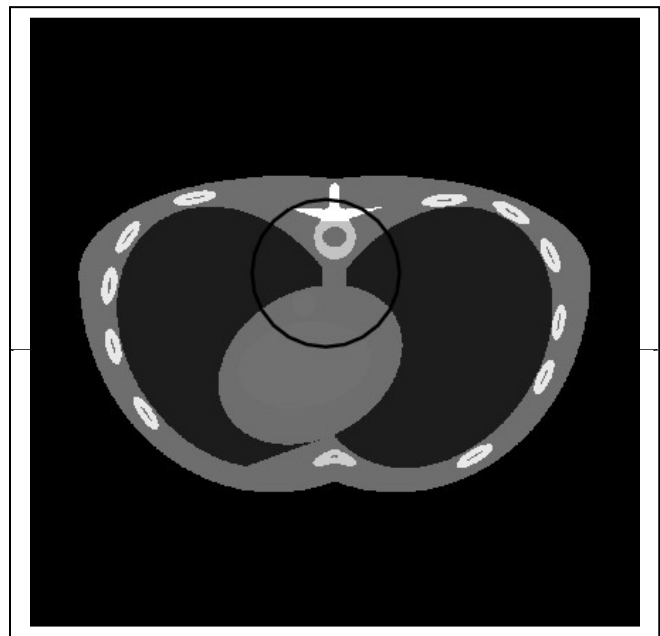


Figure 1: Modified thorax phantom with one designated RoI

Two  $1 \times 1 \text{ mm}^2$  high-contrast spots (with attenuation coefficient 18 times larger than that of its surroundings) were inserted within the RoI, see Fig. 2(b), to measure the image's point spread function. The full-width-at-half-maximum (FWHM) of the reconstructed pixels encompassing these contrast spots was taken

as a measure of the spatial resolution of the reconstructed images. The material contrast resolution,  $CR$ , of the reconstructed images was measured by distinguishing two neighboring features of nearly identical density in the reconstructed image, as quantified by [12]:

$$CR = \frac{|\mu_{RoI}^s - \mu_{RoI}^b|}{\frac{1}{2}(\sigma_{RoI}^s + \sigma_{RoI}^b)} \quad (1)$$

where  $\mu_{RoI}^s$  and  $\sigma_{RoI}^s$ , or  $\mu_{RoI}^b$  and  $\sigma_{RoI}^b$  correspond to, respectively, the mean and variance in the regions depicted in Fig. 2(b). We computed  $CR$  at two contrast-pair areas.

The modified convex maximum likelihood algorithm of [8] was used to reconstruct the full-section  $2 \times 2$  mm<sup>2</sup> coarse image. This image is not shown here as it is used only to calculate the RoI-specific projections, as explained in the above section.

The RoI-specific projections were then utilized to reconstruct the RoI image, using the same MCML algorithm, with a pixel size of  $1 \times 1$  mm<sup>2</sup>. The resulting image is shown in Fig. 2(a). For sake of comparison, the simulated actual configuration of the RoI and the RoI extracted images from full FoV FBP are shown, respectively, in Figs. 2(b), and 2(c). The full FoV FBP image was reconstructed from  $900 \times 888$  synthesized ray-sums, with added 5% noise. These ray sums were generated within a  $56^\circ$  fan-beam covering the full FoV, with 888 ray-sums in each projection and a total of 900 projections.

As Fig. 2(a) shows, the MCML image was able to resolve all main components of the thorax phantom depicted in the actual image of Fig. 2(b) and the extracted image from the full FoV FBP method shown in Fig. 2(c). The contrast resolution was even better in the MCML RoI image than in the extracted FoV FBP image, e.g. 1.0810 versus 0.1968 for the a–b contrast-pair areas, as reported in Table 1. The spatial resolution of the MCML RoI image was comparable to that of the extracted image, but more directionally dependent, as indicated in Table 1. However, in general, the MCML algorithm does not favor one direction over the

other. The overall difference between the MCML RoI reconstructed image attenuation coefficients and the actual one, calculated as a Euclidean metric,  $\delta_\mu$ , was higher than that of the extracted image (0.2591 versus 0.1411), even though there was a good matching between projections calculated from the MCML RoI reconstructed image and the input RoI-specific projections. This can be attributed to the poor sampling rate outside the RoI in narrow FoV radiation exposure and the inherent regularization of the solution introduced by the MCML algorithm.

Table 1: Contrast and spatial resolution for full field-of-view FBP and MCML RoI reconstructed images.

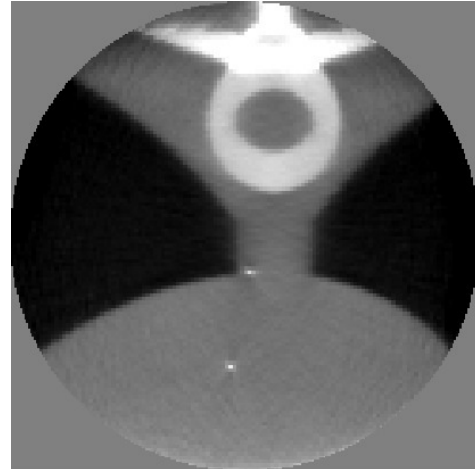
Contrast resolution ( $CR$ )		
Method	RoI of Fig 2(a)	
	Contrast pair area	
	<i>a-b</i>	<i>c-d</i>
Extracted from full field-of-view FBP	0.1968	0.1404
MCML RoI reconstructed	1.0810	3.3528
Spatial resolution (FWHM, mm)		
	RoI of Fig 2(a)	
	High Contrast Spot	
	1 <sup>st</sup>	2 <sup>nd</sup>
Extracted from full field-of-view FBP		
	x- direction	
	1.0009	1.0009
	y-direction	
	1.0054	1.0054
MCML RoI reconstructed		
	x- direction	
	1.2693	1.1510
	y-direction	
	0.9235	1.0646

## CONCLUSIONS

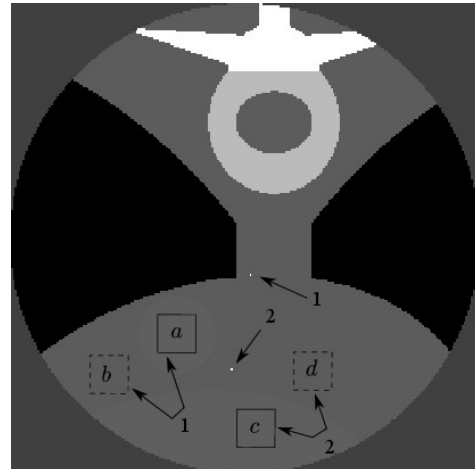
This work demonstrated that with a narrow FoV projection scheme, one can produce an RoI image without any constraints or any *a priori* information. The reconstructed RoI image in a thorax phantom was shown to be comparable in image quality to that extracted from a conventional full FoV image reconstructed with the common FBP method. Narrowing the FoV resulted in a 72% reduction in radiation exposure in the considered example.

## REFERENCES

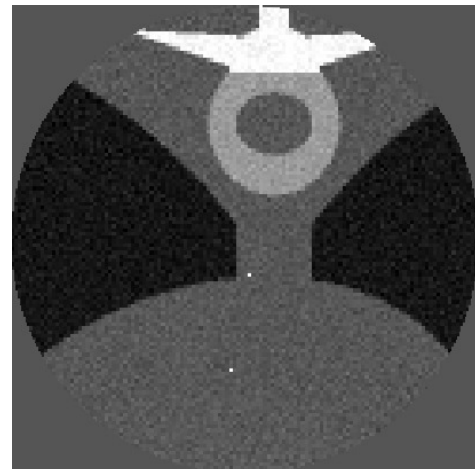
- [1] D. J. Gentle and N. M. Spyrou, Region of interest tomography in industrial applications, Nuclear Instruments and Methods in Physics Research, vol. 299(1-3), pp. 534-537, 1990.
- [2] B. Ohnesorge, T. Flohr, K. Schwarz, J. P. Heiken, and K. T. Bae, Efficient correction for CT image artifacts caused by objects extending outside the scan field of view Medical Physics, vol. 27, pp. 39-46, 2000.
- [3] D. Kolditz, Y. Kyriakou, and W. A. Kalender, Volume-of-interest (VOI) imaging in C-arm flat-detector CT for high image quality at reduced dose Medical Physics, vol. 37(6), pp. 2719-2730, 2010
- [4] Y. Shen, Y. Ying, Y. Zhong, C. J. Lai, X. Liu, Z. You, S. Ge, T. Wang, and C. C. Shaw, High resolution dual detector volume-of-interest cone beam breast CT-demonstration with a bench top system Medical Physics, vol. 38(12), pp. 6429-6442, 2011.
- [5] R. Clackdoyle, and M. Defrise, Region-of-interest reconstruction from incomplete data IEEE Signal Processing Magazine, vol. 60, pp. 60-80, 2010.
- [6] Q. Xu, X. Mou, G. Wang, J. Sieren, E. Hoffman, and H. Yu, Statistical Interior Tomography IEEE Transactions on Medical Imaging, vol. 30(5), pp. 1116-1128, 2011.
- [7] J. Hsieh, Computed Tomography; Principles, Design, Artifacts, and Recent Advances, Wiley Inter-Science, SPIE Press, Bellingham, Washington, 2009.
- [8] J. A. Fessler, E. P. Ficaro, N. H. Clinthorne, & K. Lange, Grouped-coordinate ascent algorithms for penalized-likelihood transmission image reconstruction IEEE Transaction on Medical Imaging, 1997, vol(16), pp. 166-175
- [9] A. L. Goertzen, and S. R. Cherry, Effect of phantom voxelization in CT simulations Medical Physics, vol. 29(4), pp. 492-498, 2002.
- [10] J. Fessler, Image reconstruction toolbox, <http://www.eecs.umich.edu/~fessler/code/>, Visited March 2011.
- [11] K. Sourbelle. Thorax Phantom. University of Erlangen: <http://www.imp.uni-erlangen.de/phantoms/thorax/thorax.html>, Last accessed January 02, 2011.
- [12] J. Bian, J. H. Siewerdsen, X. Han, E. Y. Sidky, J. L. Prince, C. A. Pelizzari, and X. Pan, Evaluation of sparse-view reconstruction from flat-panel-detector cone-beam CT, Physics in Medicine and Biology, vol. (55), pp. 6575-6599, 2010.



(a) The MCML RoI reconstruction from narrow field-of-view radiation exposure



(b) Actual RoI



(c) Extracted from full field-of-view filtered backprojection

Figure 2: Images of a designated RoI in the Thorax phantom of Fig. 1.